Numerical Simulation of Transient Detonation Structures in H₂-O₂ Mixtures in Smooth Pipe Bends

Ralf Deiterding

Oak Ridge National Laboratory,
P.O. Box 2008 MS6367, Oak Ridge, TN 37831, USA

1   Introduction

Accidental internal detonation waves are a common threat to the pipeline systems of petrochemical or nuclear fuel processing plants. In order to quantify the failure potential of piping structures, especially at bends, accurate detonation pressure histories are required [5]. Since detonations inhibit multi-dimensional wave structures with triple points of enhanced chemical reaction, one-dimensional detonation theory is hardly applicable. Particular for low initial pressures, resulting in large cellular structures, detonation propagation through bends is rather complex. For small radius and larger bending angle, the detonation wave structure is not maintained and triple point quenching can be observed at the outer compressive side, while detonation failure and violent re-initiation occur at the inner diffractive wall (see Fig. 5a of [7] for experimental results showing detonation re-ignition in bends).

In the present paper, we use highly resolved numerical simulations to study the transient structural evolution as low-pressure Chapman-Jouguet detonations in perfectly stirred stoichiometric hydrogen-oxygen-argon mixtures propagate through smooth two-dimensional bends. The pipes have the constant width 8 cm and encompass initially five regular detonation cells. For an unchanged inner radius of 15 cm, we consider the bending angles 15º, 30º, 45º, and 60º. The computations employ detailed chemical kinetics and have been carried out with a massively parallel high-resolution finite volume code with temporal and spatial dynamic mesh adaptation. An overview of the solution approach is given in Sec. 2. Computational results are presented and discussed in Sec. 3.

2   Numerical Model

An appropriate model for detonation propagation in premixed gases with realistic chemistry are the inviscid Euler equations for multiple thermally perfect species with reactive source terms that read

$$
\begin{aligned}
\partial_t \rho_i &+ & \nabla \cdot (\rho_i \vec{u}) &= W_i \dot{\omega}_i \,, \\
\partial_t (\rho \vec{u}) &+ & \nabla \cdot (\rho \vec{u} \otimes \vec{u}) + \nabla p &= 0 \,, \\
\partial_t (\rho E) &+ & \nabla \cdot ((\rho E + p)\vec{u}) &= 0 \,,
\end{aligned}
\tag{1}
$$

with $i = 1, \dots, K$. We assume that all K species are ideal gases in thermal equilibrium and that the hydrostatic pressure is given as the sum of the partial pressures $p_i = \mathcal{R} T \rho_i / W_i$ with $\mathcal{R}$ denoting the universal gas constant and W_i the molecular weight, respectively. The evaluation of the last equation requires the iterative calculation of the temperature T.

In here, the chemical production rates are modeled with a hydrogen-oxygen reaction mechanism extracted from the larger hydrocarbon mechanism assembled by Westbrook [8]. It consists of 34 elementary reactions and considers the 9 species H, O, OH, H₂, O₂, H₂O, HO₂, H₂O₂ and Ar. A time-operator splitting approach is employed to decouple hydrodynamic transport and chemical reaction numerically.

Figure 1: Schlieren plot of density on triple point tracks (left) and on refinement regions (shaded gray, middle and right) for $\varphi = 45^{\circ}$ after $t = 150\,\mu$s simulated time.

A semi-implicit scheme for ordinary differential equations is used to integrate the reactive source terms locally in each finite volume cell. Temperature-dependent material properties are taken from look-up tables that are constructed during start-up of the computational code. The reaction rate expressions are evaluated by a Fortran-77 function, which is produced by a source code generator on top of the Chemkin-II library in advance.

Since detonations involve shock waves, we use a finite volume discretization with proper upwinding in all characteristic fields. The scheme utilizes a quasi-one-dimensional approximate Riemann solver of Roe-type and is extended to multiple space-dimensions via the method of fractional steps. Special corrections are applied to avoid unphysical total densities and internal energies near vacuum, to ensure positive mass fractions, and to prevent the disastrous carbuncle phenomenon. The MUSCL (Monotone Upstream-centered Schemes for Conservation Laws) variable extrapolation technique is employed to construct a second-order scheme. Geometrically complex boundaries are considered by using some of the Cartesian finite volume cells to enforce immersed boundary conditions. Their values are set immediately before the original Cartesian numerical update to model rigid embedded walls. A detailed description of the boundary incorporation for system (1) can be found in [2]; the upwind scheme including all modifications is detailed in [1, 3]. To accommodate the disparate scales in detonation wave simulation effectively, the upwind scheme is incorporated into a dynamic block-structured adaptive mesh refinement (SAMR) method for hyperbolic equations. The SAMR implementation has been parallelized with the MPI library for distributed memory machines. See [2] for details.

3   Computational results

Computational model and numerical solution algorithm have been verified and validated meticulously in [1]. For the frequently studied case of a regularly oscillating Chapman-Jouguet detonation in a mixture of $2\,H_2 + O_2 + 7\,Ar$ with initial pressure $6.67\,$kPa and temperature $293\,$K, our computational model predicts an undisturbed cell width of $\sim 30\,$mm, which is in perfect agreement with other computations [4, 6] and close to the carefully derived experimental result of $38 \pm 8\,$mm given in [6].

In this paper, we consider the same detonation configuration, but increase the initial pressure slightly to $10.0\,$kPa. The one-dimensional detonation structure theory after Zel'dovich, von Neumann, and Döring (ZND) predicts a detonation velocity of $1638.5\,$m/s, a von Neumann Pressure of $\sim 270\,$kPa, and a reaction length of $l_{ig} \approx 0.878\,$mm for this case. We place the ZND solution in a two-dimensional straight channel and perturb it slightly to compute a regularly oscillating solution with undisturbed detonation cell width of $\sim 16\,$mm. A snapshot of a single cell of this regular solution is reproduced periodically and used to initialize the flow field with the detonation front approximately $13\,$cm before the beginning of the curved pipeline section.

In previous investigations [3], it was found that for the reaction network considered in here, a spatial resolution of minimally $6\,\mathrm{Pts}/l_{ig}$ is necessary to resolve all intermediate reaction products in the
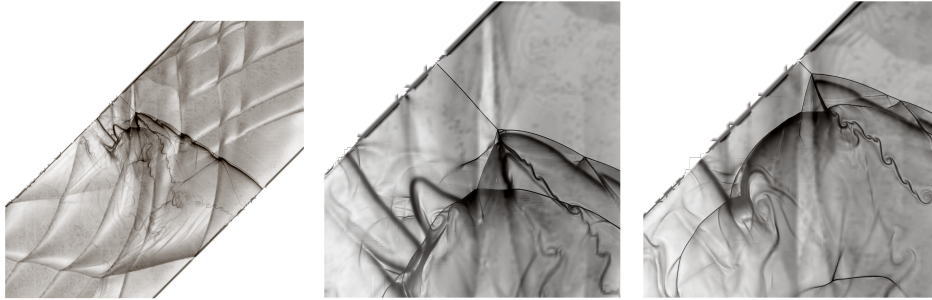
Figure 2: Schlieren graphics of the density on top of triple point tracks for $\varphi = 45^{\circ}$ show the transverse detonation wave after $t = 210\,\mu$s (left and middle) and $t = 217\,\mu$s (right) simulated time. The secondary triple point propagating along the transverse detonation wave is clearly visible in the enlargements.

one-dimensional ZND solution accurately. Around multi-dimensional triple points, however, a higher resolution is required to capture the internal wave structure completely. Our previous two-dimensional verification simulations for the regularly oscillating case used effective resolutions up to $44.8\,\mathrm{Pts}/l_{ig}$, which is sufficient to resolve even secondary triple points reliably (cf. [1]). Note that for such high local resolutions, only a very carefully reduced multi-step reaction mechanism can be expected to lead to results equivalent to full chemistry. Because of the moderate computational expense of hydrogen-oxygen chemistry, we prefer to employ the full chemical kinetic model instead.

In order to accommodate a reduction of the induction length when the detonation wave gets compressed, all computations throughout this paper use an effective resolution of $67.6\,\mathrm{Pts}/l_{ig}$, which is achieved by four additional levels of Cartesian mesh adaptation with refinement factors 2, 2, 2, and 4. A physically motivated combination of scaled gradients of pressure and density and heuristically estimated relative errors in the mass fractions is applied as adaptation criteria (c.f. [1]). For instance, for bend angle $\varphi = 60^{\circ}$, with a base mesh of 1200×992 cells, the adaptive computation uses approximately 7.1 M to 3.4 M cells on all and 4.8 M to 1.8 M cells on the highest level instead of $\sim 1,219$ M in the uniform case. The calculations were run on 64 dual-processor nodes of the Advanced Simulation and Computing (ASC) Linux cluster at Lawrence Livermore National Laboratory and required nevertheless $\sim 70,000$ h CPU each (approximately 23 days wall clock time). The extraordinary high efficiency in capturing only the essential features near the detonation front is illustrated in Fig. 1, in which the characteristic double Mach reflection pattern (cf. [4, 1]) around primary triple points is clearly resolved. Note that the reaction zone appears in Figs. 1 and 2 as the diffused black line following the sharp shock wave at the head of the detonation front.

Detonation propagation through a bend is a combined process that involves detonation wave reflection and diffraction. At the outer wall, the detonation becomes overdriven as the leading shock front undergoes Mach reflection. Along the inner wall, shock wave diffraction causes a continuous pressure decrease that results in a slight temporary increase in detonation cell size for a bending angle of $\varphi = 15^{\circ}$, in a transmitted marginal detonation close to the limit of detonability for $\varphi = 30^{\circ}$, and in temporary detonation failure for $\varphi \geq 45^{\circ}$. For $\varphi \geq 30^{\circ}$, the appearance of unreacted pockets behind the marginal detonation wave can be observed (see Fig.1). For the completely transmitted marginal case ($\varphi = 30^{\circ}$), the transition back to a regular oscillation is initiated by a strong triple point originating in the region of detonation Mach reflection. For the configurations with $\varphi \geq 45^{\circ}$, in which additionally partial detonation failure occurs, the transverse re-initiation wave itself becomes a detonation. It propagates in the direction normal to the pipe middle axis and causes severe loading conditions when it impinges on the inner wall. As the transverse detonation travels inward, an instationary triple point arises on the transverse detonation itself that propagates toward the primary detonation front. The two right graphics of Fig. 2 display this triple point and its trajectory. Peak pressures of more than $1.2\,\mathrm{MPa}$ occur in the vicinity of this triple point. When it hits the inner wall, short-term pressures $> 3.4\,\mathrm{MPa}$ do arise. For $\varphi = 60^{\circ}$, the reflection of the transverse wave is less violent since the critical triple point merges
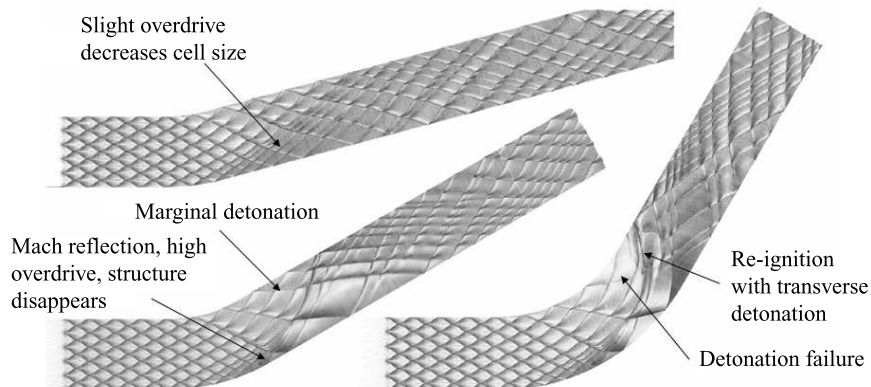
Figure 3: Triple point tracks for $\varphi = 15^{\circ}$ (left, top), $\varphi = 30^{\circ}$ (left, bottom), and $\varphi = 60^{\circ}$ (right).

with the primary triple point at the detonation front before wall contact. Figure 3 shows triple point records (based on maximal vorticity) numerically derived during the computations that correspond to smoke foil tracks in experiments. The main stages of detonation transmission are indicated.

The given analysis underlines the importance of the accurate consideration of transverse detonation structures in numerical simulations used for plant safety analysis. Computations on significantly coarser meshes that fail to resolve the detonation structure evolution are inherently unable to predict the re-ignition event correctly and are therefore likely to severely underestimate the maximal pressures and reaction rates of a given setup.

Acknowledgments

References

[1] R. Deiterding. *Parallel adaptive simulation of multi-dimensional detonation structures.* PhD thesis, Brandenburgische Technische Universität Cottbus, Sep 2003.

[2] R. Deiterding. Dynamically adaptive simulation of regular detonation structures using the Cartesian mesh refinement framework AMROC. *Int. J. Computational Science Engineering*, 2007. In press.

[3] R. Deiterding and G. Bader. High-resolution simulation of detonations with detailed chemistry. In G. Warnecke, editor, *Analysis and Numerics for Conservation Laws*, pages 69–91. Springer, 2005.

[4] X. Y. Hu, B. C. Khoo, D. L. Zhang, and Z. L. Jiang. The cellular structure of a two-dimensional $H_2/O_2/Ar$ detonation wave. *Combustion Theory and Modelling*, 8:339–359, 2004.

[5] M. A. Nettleton. Recent work on gaseous detonation. *Shock Waves*, 12:3–12, 2002.

[6] F. Pintgen, C. A. Eckett, J. M. Austin, and J. E. Shepherd. Direct observations of reaction zone structure in propagating detonations. *J. Combust. Flame*, 133:211–229, 2003.

[7] G. O. Thomas and R. L. Williams. Detonation interaction with wedges and bends. *Shock Waves*, 11:481–492, 2002.

[8] C. K. Westbrook. Chemical kinetics of hydrocarbon oxidation in gaseous detonations. *J. Combust. Flame*, 46:191–210, 1982.